

Optimising hadronic collider simulations using amplitude neural networks

Ryan Moodie

Institute for Particle Physics Phenomenology, Ogden Centre for Fundamental Physics,
Department of Physics, University of Durham, South Road, Durham, DH1 3LE, UK

E-mail: ryan.i.moodie@durham.ac.uk

Abstract. Precision phenomenological studies of high-multiplicity scattering processes at collider experiments present a substantial theoretical challenge and are vitally important ingredients in experimental measurements. Machine learning technology has the potential to dramatically optimise simulations for complicated final states. We investigate the use of neural networks to approximate matrix elements, studying the case of loop-induced diphoton production through gluon fusion. We train neural network models on one-loop amplitudes from the `NJet C++` library and interface them with the `Sherpa` Monte Carlo event generator to provide the matrix element within a realistic hadronic collider simulation. Computing some standard observables with the models and comparing to conventional techniques, we find excellent agreement in the distributions and a reduced total simulation time by a factor of thirty.

1. Introduction

With the increasing Large Hadron Collider dataset driving ever more precise experimental measurements, Standard Model (SM) predictions for high-multiplicity scattering at hadronic colliders form a vital part of precision phenomenology studies. Currently, these calculations mainly rely on automated numerical codes [1] to calculate high-multiplicity matrix elements, including tree-level real corrections at next-to-leading order (NLO) and double-real corrections at next-to-next-to-leading order (NNLO), and one-loop real-virtual corrections at NNLO. These codes have been a theoretical revolution, particularly at one-loop, but the evaluation time is relatively high. Due to the high dimensionality of the phase space, these corrections are often the computational bottleneck in higher-order calculations.

Following recent advances in precision QCD, there has been a flurry of activity around NNLO QCD corrections to diphoton-plus-jet production, including full-colour two-loop amplitudes [2] and leading-colour NNLO distributions [3]. In the loop-induced gluon fusion channel, the full-colour two-loop amplitudes were computed [4], leading to full-colour NLO distributions [5]. Also for diphoton production through gluon fusion, the three-loop amplitudes were calculated [6], making available the final remaining piece for its NNLO corrections. Therefore, we study the loop-induced class of processes with two photons and many gluons as they are extremely relevant for current phenomenology.

Machine learning (ML) technology has found a wealth of application in high energy physics [7]. We employ the ensemble neural network (NN) model of Ref. [8], which studied e^+e^- annihilation to jets, to emulate the gluon-initiated diphoton amplitudes within a full Monte Carlo (MC) event generator simulation. This tests the methodology against the additional complexity of

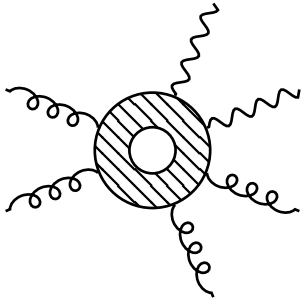


Figure 1. Diagram of $gg \rightarrow \gamma\gamma gg$ ($N = 6$) at LO. The photons couple to an internal quark loop.

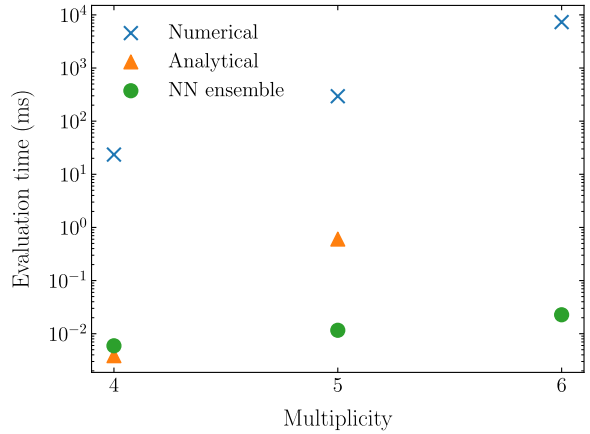


Figure 2. Single-threaded CPU evaluation time of the matrix element for a single phase space point. The value is the mean of 100 evaluations over a random phase space. Results are shown for available implementations at various multiplicities, including numerical and analytical evaluations using `NJet` and inference on the NN model.

hadronic collider simulations, including parton distribution function (PDF) convolution and variable centre-of-mass scales, complex phase space cuts and jet clustering, and phase space sampling optimisation methods of integrators.

This contribution is organised as follows. We first discuss the gluon-initiated diphoton amplitudes and their implementations within the C++ `NJet` library [9, 10] which were used for training. We then describe the phase space partitioning used to handle infrared (IR) divergent regions. Next, we present the architecture of the NNs used. Then, we discuss the simulation pipeline and interface of the NN model to the `Sherpa` MC event generator [11]. Finally, we study the performance of the model compared to the original amplitude library for $gg \rightarrow \gamma\gamma gg$ and present some distributions before concluding.

This contribution is based on Ref. [12]. Our code is publicly available [13].

2. Amplitudes

As there is no vertex coupling gluons to photons in the SM, diphoton-plus-jets production through gluon fusion (Fig. 1) is loop induced. The leading order (LO) process is $\mathcal{O}(\alpha_s^{N-2})$ for multiplicity N , appearing at NNLO in the perturbative expansion of the combined quark- and gluon-initiated process. We study the channels with only gluons and photons in the external particles, $gg \rightarrow \gamma\gamma + n \times g$. These proceed through a quark loop at LO.

Conventional event generator simulations optimise virtual corrections in NLO calculations by learning the phase space of the LO process and using this to sample the virtual contribution. This technique fails for loop-induced processes, where the expensive one-loop amplitude has no tree-level process to optimise the phase space on. Therefore, new methods are required to improve the efficiency of integrating these channels at high multiplicity.

We use amplitudes from the `NJet` library. These include two classes: an automated numerical setup for arbitrary multiplicity; and hard-coded analytical expressions for $N \in \{4, 5\}$. The numerical implementation obtains the diphoton amplitudes by summing permutations of pure-

gluon primitive amplitudes [14], which are themselves based on generalised unitary [15] and integrand reduction [16]. While completely automated, evaluation time and numerical stability are increasingly difficult to control. The hard-coded implementations offer compact analytical expressions with extremely fast and stable evaluation, although they are unavailable for higher multiplicity. The $N = 5$ result is obtained through a finite field reconstruction [17]. The evaluation timings of these methods are compared to the NN model in Fig. 2.

3. Phase space partitioning

Training a single NN over the entire phase space results in a poor fit, especially at higher multiplicity [8]. This is caused by regions where the amplitude becomes IR divergent, which arise from soft (s_i) and collinear (c_{ij}) emissions. These singularities are regulated with cuts, but the local regions exhibit extreme curvature which causes problems for the global fit. Therefore, we train a separate NN on each of the IR structures of the phase space.

We first partition the phase space into a non-divergent region, $\mathcal{R}_{\text{non-div}}$, and a divergent region, \mathcal{R}_{div} . We select into \mathcal{R}_{div} by a cut, $\min(\{s_{ij}/s_{12} : i, j \in [1, N]\}) < y$. The threshold y must be tuned to discriminate points of similar scales into each region, while having sufficient points in \mathcal{R}_{div} to train on.

We then sub-divide \mathcal{R}_{div} according to the decomposition of the FKS subtraction scheme [18]. This defines a set of FKS pairs, $\mathcal{P}_{\text{FKS}} = \{(i, j) : s_i \vee s_j \vee c_{ij}\}$, corresponding to the $\binom{N}{2} - 1$ singular configurations, which includes redundancy (App. B of Ref. [8]). Each pair is assigned a partition function, $\mathcal{S}_{ij} = 1/\left(s_{ij} \sum_{j, k \in \mathcal{P}_{\text{FKS}}} 1/s_{jk}\right)$, which smoothly isolates that divergence on multiplication with the matrix element.

We train a NN on $|\mathcal{A}(\mathbf{p})|^2$ for $\mathbf{p} \in \mathcal{R}_{\text{non-div}}$, and a NN on each of the partition-function-weighted matrix elements, $\{\mathcal{S}_{ij} |\mathcal{A}(\mathbf{p})|^2 : i, j \in \mathcal{P}_{\text{FKS}} ; \mathbf{p} \in \mathcal{R}_{\text{div}}\}$. We reconstruct the complete matrix element in \mathcal{R}_{div} by summing the weighted matrix elements, $|\mathcal{A}|^2 = \sum_{i, j \in \mathcal{P}_{\text{FKS}}} \mathcal{S}_{ij} |\mathcal{A}|^2$. This ensemble of NNs, referred to as the model, can be used to accurately infer the matrix element over the complete phase space.

Note that increasing the cut y incurs a performance penalty due to the higher cost of inferring over several NNs in \mathcal{R}_{div} compared to the single NN in $\mathcal{R}_{\text{non-div}}$.

4. Model architecture

Although using fine-tuned architectures for each configuration (process, cuts, etc.) would provide optimal performance, this would be prohibitively expensive. We use a general setup as this is more practical in real-world application, performing hyperparameter optimisation on the $gg \rightarrow \gamma\gamma g$ process.

Each NN uses a fully-connected architecture, parameterised using the Keras Python interface [19] to the TensorFlow ML library [20]. There are $4 \times N$ input nodes: one for each component of each momentum in the phase space point. The three hidden layers are comprised of 20, 40, and 20 nodes respectively, all with hyperbolic-tangent activation functions. There is a single output node with a linear activation function, which returns the approximation of the matrix element.

We train with a mean-squared-error loss function, using Adam-optimised stochastic gradient descent [21]. The number of training epochs is determined by Early Stopping regularisation, with a patience of 100 epochs to mitigate the effects of the limited number of divergent points that may appear in the validation set. We use 32-bit floating-point numbers throughout.

5. Pipeline

Our ML pipeline for the $gg \rightarrow \gamma\gamma gg$ results presented is: generate the training and validation datasets by running **Sherpa** with **NJet** on a unit integration grid; train the model; infer on the

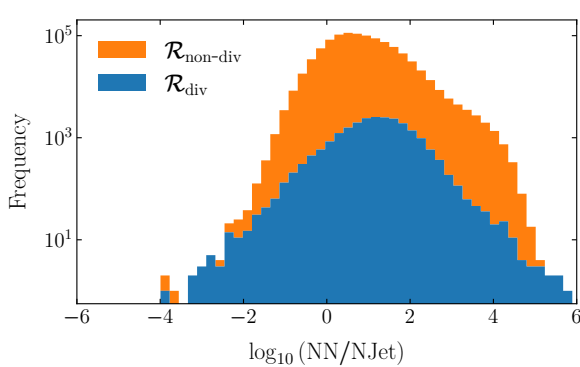


Figure 3. Stacked histogram by region of the logarithm of the ratio between the matrix element returned by the model and `NJet` for each point in a 1M subset of the training data for $gg \rightarrow \gamma\gamma gg$. The region cut is $y = 10^{-3}$ and \mathcal{R}_{div} contains 2.4% of the points.

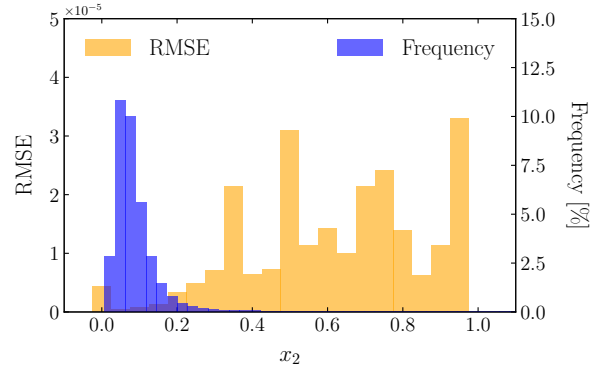


Figure 4. Histogram of the root mean squared error (RMSE) of the model compared to `NJet` for a univariate slice of phase space in x_2 , the momentum fraction of the second outgoing particle (photon), for $gg \rightarrow \gamma\gamma g$. Also shown are the points in the training dataset, binned in x_2 .

model to estimate the matrix elements during event generation with `Sherpa`, using the same integration grid.

Input data consists of a list of phase space points, $p_i^\mu \in \mathbb{R}^{4N}$, and the corresponding colour- and helicity-summed one-loop squared amplitude, $|\mathcal{A}|^2 \in \mathbb{R}$. Phase space sampling is determined by the integrator, so we train for a specific integrator. The data is extracted from a run of the integrator, generating 100k points which are split 4:1 into training and validation datasets. A 3M point testing dataset is produced by a second run of the integrator with a different random number seed and used to evaluate model performance.

We infer on an ensemble of 20 models, each of which have different random weight initialisation and shuffled training and validation datasets. We take as the result the mean of the ensemble, with the standard error providing the precision/optimality error [8].

While training was performed using `Python`, event generators are generally written in `C++`. To use the model within a simulation, we wrote a `C++` inference code and bespoke `C++` interface to `Sherpa` for the inference code. The weights of the trained models are written to file and read by the inference code at runtime; the library `Eigen` [22] is used to perform efficient linear algebra on the CPU. The interface can also be used to call `C++` amplitude libraries; we use this to interface `NJet` to `Sherpa` to generate the datasets, which is performed with 64-bit floats.

PDFs are provided by LHAPDF [23] using the NNPDF3.1 set `NNPDF31_nlo_as_0118` [24]. Cuts are adapted from those in Ref. [25]. Analysis is performed using `Rivet` [26] with an adapted reference analysis script [27].

6. Results

Comparing the output of the trained model to the amplitude library value by point-by-point ratio in Fig. 3, we see an approximate Gaussian error distribution with a shifted mean in both regions. Both region histograms have a similar mean, indicating comparable fitting performance. $\mathcal{R}_{\text{non-div}}$ shows a bump on the right, although suppressed by two orders of magnitude compared to the peak, which arises from points near the cutoff y .

Despite the per-point agreement being somewhat poor, the total cross section is found to be in agreement, with $\sigma_{\text{NN}} = (4.5 \pm 0.6) \times 10^{-6} \text{ pb}$ (MC error) and $\sigma_{\text{NJet}} = (4.9 \pm 0.5) \times 10^{-6} \text{ pb}$

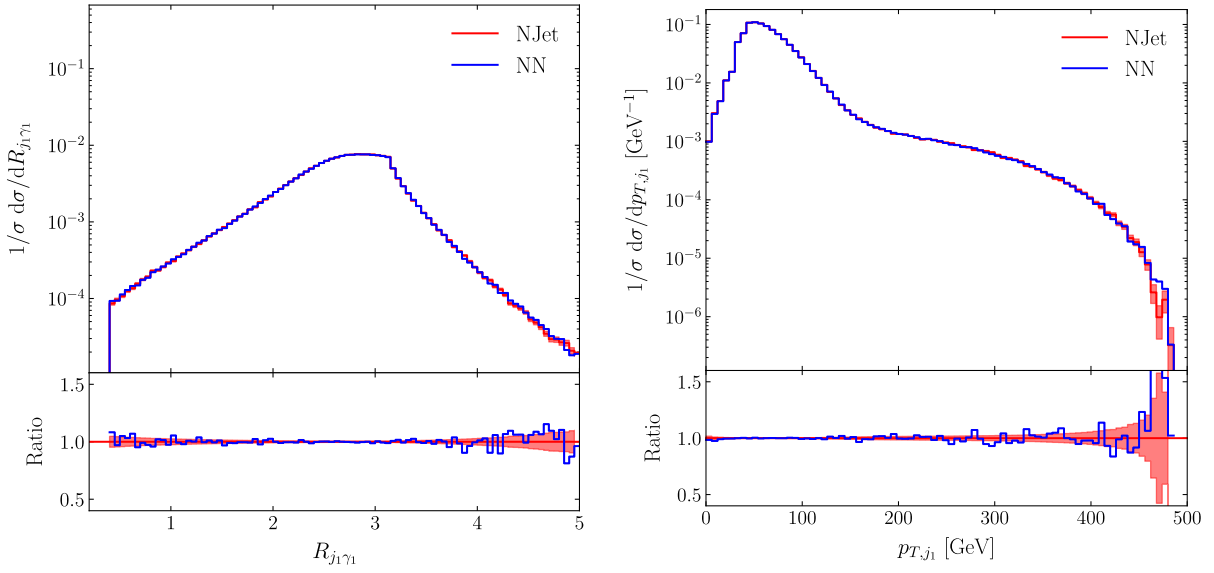


Figure 5. Differential normalised cross sections for $gg \rightarrow \gamma\gamma gg$, comparing **NJet** (MC error) to the model (precision/optimality error), in R-separation between the hardest jet and photon (left) and the transverse momentum of the hardest jet (right). Refer to Ref. [12] for definitions of observables and cuts, and further distributions.

(precision/optimality error). This is perhaps not surprising as it is a well known fact in ML that the networks learn the mean of the target distribution when using a mean squared loss function (App. A of Ref. [8]). In addition, Fig. 4 shows that the regions that are sampled the most due to the shape of the gluon PDF are those that have the lowest error. This indicates that the accuracy of distributions inferred with the model is dependent on the choice of process, cuts, and observable.

Ref. [28] achieves improved per-point agreement at tree-level by exploiting the factorisation properties of matrix elements.

Fig. 5 shows excellent agreement between the distributions obtained from the model and **NJet** for two differential slices of phase space. There are some fluctuations in the tails although they appear statistical rather than systematic and the model predictions mostly remain within the **NJet** MC error bands. Normalised NN uncertainties are negligible compared to the MC error.

Ref. [12] also demonstrates how agreement can be improved in \mathcal{R}_{div} by reweighting event weights by the ratio of the emulated and true matrix elements at known points from the training data, as well as showing good performance for $gg \rightarrow \gamma\gamma g$ when relaxing cuts at inference compared to training.

7. Conclusion

We extend previous work which pioneered the emulation of scattering amplitudes with NNs, studying these techniques for the first time within a full hadronic collider simulation. We focus on loop-induced diphoton-plus-jet production via gluon fusion. The difficulties introduced by IR behaviour are tamed by partitioning the phase space as prescribed by FKS subtraction. We provide a general interface for trained models to **Sherpa**.

We find that amplitude NN models provide an efficient and general framework for optimising high-multiplicity observables at hadronic colliders. Agreement in differential distributions is excellent. As the cost of inference is negligible compared to the amplitude library call in training, the speed up in total simulation time (including training) compared to conventional methods

is given by the ratio of the number of points used for inference and training, $N_{\text{infer}}/N_{\text{train}}$. For this study, this gave a factor of thirty, although for studies with higher statistics or coverage of multiple cut configurations, the factor would be much greater.

Acknowledgments

I would like to thank Joseph Aylett-Bullock and Henry Truong for useful discussions, and Simon Badger for comments on the draft manuscript. I am supported by UKRI-STFC ST/S505365/1 and ST/P001246/1.

References

- [1] Degrande C, Hirschi V and Mattelaer O 2018 *Ann. Rev. Nucl. Part. Sci.* **68** 291–312
- [2] Agarwal B, Buccioni F, von Manteuffel A and Tancredi L 2021 *Phys. Rev. Lett.* **127** 262001 (*Preprint* 2105.04585)
- [3] Chawdhry H A, Czakon M, Mitov A and Poncelet R 2021 *JHEP* **09** 093 (*Preprint* 2105.06940)
- [4] Badger S *et al.* 2021 *JHEP* **2021** (*Preprint* 2106.08664)
- [5] Badger S, Gehrmann T, Marcoli M and Moodie R 2022 *Phys. Lett. B* **824** 136802 (*Preprint* 2109.12003)
- [6] Bargiela P, Caola F, von Manteuffel A and Tancredi L 2021 (*Preprint* 2111.13595)
- [7] Feickert M and Nachman B 2021 (*Preprint* 2102.02770)
- [8] Badger S and Bullock J 2020 *JHEP* **06** 114 (*Preprint* 2002.07516)
- [9] Badger S, Biedermann B, Uwer P and Yundin V 2013 *Comput. Phys. Commun.* **184** 1981–1998 (*Preprint* 1209.0100)
- [10] Badger S, Biedermann B, Uwer P and Yundin V 2014 *J. Phys. Conf. Ser.* **523** 012057 (*Preprint* 1312.7140)
- [11] Bothmann E *et al.* (Sherpa) 2019 *SciPost Phys.* **7** 034 (*Preprint* 1905.09127)
- [12] Aylett-Bullock J, Badger S and Moodie R 2021 *JHEP* **2021** (*Preprint* 2106.09474)
- [13] Aylett-Bullock J and Moodie R 2021 n3jet_diphoton v1 https://gitlab.com/JosephPB/n3jet_diphoton
- [14] de Florian D and Kunszt Z 1999 *Phys. Lett. B* **460** 184–188 (*Preprint* hep-ph/9905283)
- [15] Badger S D 2009 *JHEP* **01** 049 (*Preprint* 0806.4600)
- [16] Ossola G, Papadopoulos C G and Pittau R 2007 *Nucl. Phys. B* **763** 147–169 (*Preprint* hep-ph/0609007)
- [17] Peraro T 2019 *JHEP* **07** 031 (*Preprint* 1905.08019)
- [18] Frederix R, Frixione S, Maltoni F and Stelzer T 2009 *JHEP* **10** 003 (*Preprint* 0908.4272)
- [19] Chollet F *et al.* 2015 Keras <https://github.com/fchollet/keras>
- [20] Abadi M *et al.* 2015 TensorFlow <https://www.tensorflow.org/>
- [21] Kingma D P and Ba J 2015 *3rd International Conference for Learning Representations* (*Preprint* 1412.6980)
- [22] Guennebaud G, Jacob B *et al.* 2010 Eigen v3 <https://eigen.tuxfamily.org>
- [23] Buckley A *et al.* 2015 *Eur. Phys. J. C* **75** 132 (*Preprint* 1412.7420)
- [24] Ball R D *et al.* (NNPDF) 2017 *Eur. Phys. J. C* **77** 663 (*Preprint* 1706.00428)
- [25] Badger S, Guffanti A and Yundin V 2014 *JHEP* **03** 122 (*Preprint* 1312.5927)
- [26] Bierlich C *et al.* 2020 *SciPost Phys.* **8** 026 (*Preprint* 1912.05451)
- [27] Aaboud M *et al.* (ATLAS) 2017 *Phys. Rev. D* **95** 112005 (*Preprint* 1704.03839)
- [28] Maître D and Truong H 2021 *JHEP* **11** 066 (*Preprint* 2107.06625)